Available online at www.sciencedirect.com
ScienceDirect
Dyes and Pigments 77 (2008) 210–216
DYES and PIGMENTS
www.elsevier.com/locate/dyepig

Yellow $Zn_xNi_{1-x}WO_4$ pigments obtained using a polymeric precursor method

André Luiz M. de Oliveira [a], Jailson M. Ferreira [a,b], Márcia R.S. Silva [a], Glauco S. Braga [a], Luiz E.B. Soledade [a], M.A. Maurera Maria Aldeiza [a], Carlos A. Paskocimas [c], Severino J.G. Lima [d], Elson Longo [e], Antonio Gouveia de Souza [a], Iêda M. Garcia dos Santos [a,*]

[a] *Laboratório de Combustíveis e Materiais, Depto. de Química, Centro de Ciências Exatas e da Natureza, UFPB, Campus 1, Cidade Universitária, CEP 58059900, João Pessoa, PB, Brazil*
[b] *COAMA, Centro Federal de Educação Tecnológica da Paraíba, João Pessoa, PB, Brazil*
[c] *Departamento de Engenharia Mecânica, UFRN, Natal, RN, Brazil*
[d] *Depto. de Tecnologia Mecânica, UFPB, João Pessoa, PB, Brazil*
[e] *CMDMC, UNESP, Araraquara, SP, Brazil*

Received 6 February 2007; received in revised form 10 May 2007; accepted 15 May 2007
Available online 25 May 2007

Abstract

New tungstate-based ceramic pigments, displaying $Zn_xNi_{1-x}WO_4$ stoichiometry, were obtained at low temperature using a polymeric precursor method. The powder precursors were milled in an attritor mill in an alcoholic medium and heat treated for 12 h, yielding homogeneous and crystalline powder pigments. Characterization (TG/DTA, XRD, IR and colorimetry) showed that mass loss increased with increasing Zn contents. Despite the presence of secondary phases and impurities, the wolframite phase was present in all samples. IR analysis revealed bands related to Me–O and $[WO_6]^{6-}$ group stretching was observed. The intensity of the yellow color of the pigments increased with increasing amount of nickel.

Keywords: Wolframite; Yellow pigments; Tungstate; Absorbance; Colorimetry

1. Introduction

Tungstates are widely studied due to the high technological interest related to their important physical and chemical properties [1,2]. For instance, their excellent photochromic and electrochromic properties are commonly used in smart windows and information storage devices; they are also used as photoanodes, fluorescent lamps, optical fibers, catalysis, image tubes for television, scintillators in radiological systems and as ceramic pigments [1].

Inorganic pigments are widely used in various areas such as paints, ceramics, plastics, glazes and glasses, despite being, in some cases, toxic. Despite the relatively few number of tungstates used as pigments, the colors of these materials are suitable for their use in paints [3,4].

Depending on the size of the modifier cation, tungstates can crystallize in either scheelite or wolframite form. The major natural tungsten ores contain the minerals scheelite, $CaWO_4$ and wolframite, (Fe, Mn)WO_4 [5]. Scheelite structures, with the tungsten in tetrahedral coordination, are formed when large bivalent cations (Ca^{2+}, Ba^{2+}, Pb^{2+} and Sr^{2+}) are present; in the cases of smaller bivalent cations (Fe^{2+}, Mn^{2+}, Co^{2+}, Ni^{2+}, Mg^{2+} and Zn^{2+}) the wolframite structure is formed, with the tungsten in octahedral coordination [5]. In addition,

* Corresponding author. Tel./fax: +55 83 32167441.
E-mail address: ieda@quimica.ufpb.br (I.M. Garcia dos Santos).

0143-7208/$ - see front matter © 2007 Elsevier Ltd. All rights reserved.
doi:10.1016/j.dyepig.2007.05.004

the transition from scheelite to wolframite can be stimulated by high pressure, ~1.2 GPa for $CaWO_4$ and 5 GPa for $BaWO_4$ [6]. The scheelite structure is characterized by tetragonal space group $I4_1/a$ or C_{4h}^6 [7–8] and may be regarded as a cubic close-packed array of A^{2+} and $[WO_4]^{-2}$ units with coordination numbers of 8 and 4 oxygen atoms for the A and W cations, respectively. The wolframite structure is characterized by the monoclinic space group $P2/c$ or C_{2h}^4, with the A and the W cations in octahedral symmetry [7,8].

Several synthetic methods have gained popularity for the preparation of fine ceramic oxide powders namely, the sol–gel, co-precipitation, hydrothermal, citrate gel and other gel-combustion methods [9]. The chemical and physical properties of metal oxides, including tungsten oxides, depend on the synthetic route employed.

In this work, tungstates were synthesized using a polymeric precursor method, which is characterized by high reproducibility and low cost, compared to other chemical methods of synthesis. The method has been successfully used in the synthesis of nanoparticles and thin films of different oxides and is based on the chelation of cations by a hydrocarboxylic acid (normally citric acid), followed by polyesterification using a glycol (normally ethylene glycol) [10]. The formed precursor resins contain cations randomly distributed throughout the polymer [11].

In this work, $Zn_xNi_{1-x}WO_4$ tungstates were synthesized and characterized using TG/DTA, XRD, IR and visible reflectance spectroscopy. The influences of temperature and the network modifier on the thermal, structural and optical properties of the pigments were investigated.

2. Experimental procedure

For the synthesis of the $Zn_xNi_{1-x}WO_4$ ($x = 0$, 0.2, 0.4, 0.6, 0.8, 1) pigments, the polymeric precursor method, elsewhere detailed [12–14], was employed. A tungsten citrate solution was initially prepared, followed by the synthesis of the powder precursor.

Preparation of the tungsten citrate solution started with the dissolution of tungstic acid in distilled water, at 70 °C, at pH of 7–8. Citric acid was dissolved in distilled water at the same temperature and this solution was slowly added to the tungstic acid solution. The ensuing tungsten citrate solution was later filtered and subjected to a gravimetric analysis, in order to obtain information concerning stoichiometry.

For the synthesis of the polymeric resin, citric acid was added to the tungsten citrate solution, followed by the addition of nickel or zinc salt, under constant mixing and at a temperature of ~100 °C. The ensuing resins were calcined at 300 °C for 1 h, leading to the formation of powder precursors which were deagglomerated and milled in an attritor mill for 4 h, in an aqueous CH_3OH medium. The precursors were then calcined at 350 °C for 12 h, to burn-off the organic matter. The powders were then characterized using thermal analysis (TG/DTA) (SDT 2980 – TA Instruments) employing air with a flow rate of 110 ml min^{-1} and a heating rate of 10 °C/min up to 900 °C.

The precursors were subsequently calcined in air, at 400, 500, 600 and 700 °C for 2 h, and characterized by infrared spectroscopy (IR), X-ray diffraction (XRD) and visible reflectance spectroscopy. IR analyses were performed using an MB-102 Bomem spectrophotometer, in the range of 400–2000 cm^{-1}, using KBr pellets while XRD patterns were obtained using a D-5000 Siemens diffractometer, employing Kα Cu radiation. The visible reflectance spectroscopy was carried out using a Gretag Macbeth Color-Eye 2180 colorimeter, under D_{65} using d/8° viewing, with specular reflectance excluded.

3. Results and discussion

The TG and DTA curves of the precursors, after milling and pre-treatment in an oxygen atmosphere, are presented in Fig. 1. In all samples, the thermal decomposition occurred in

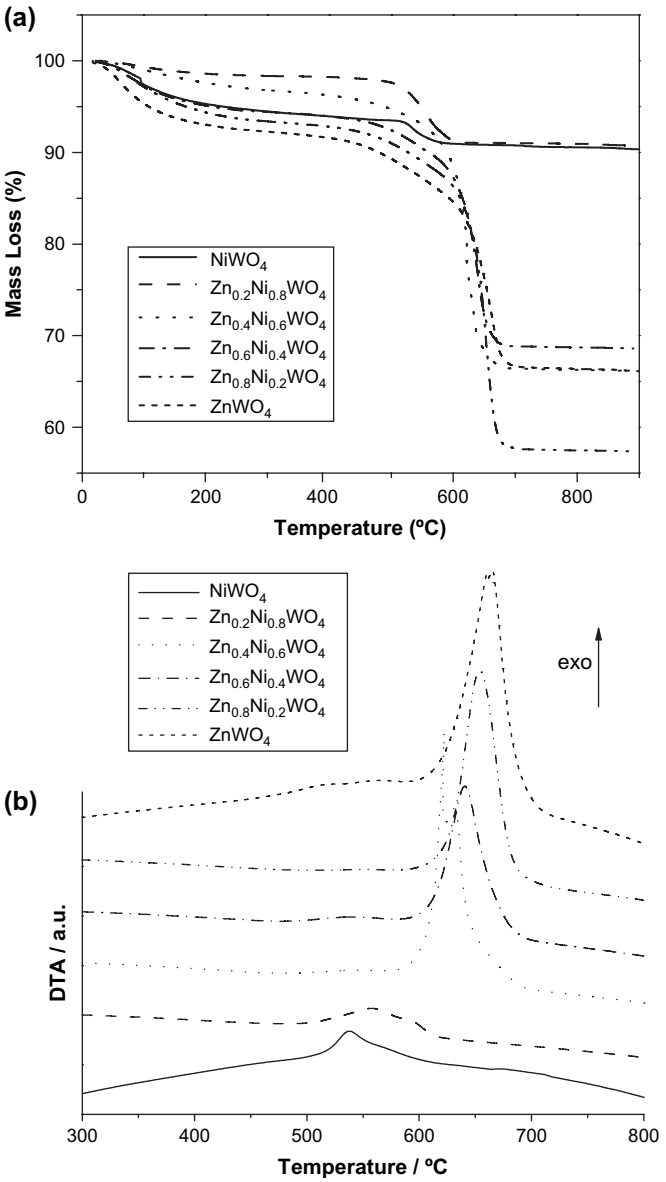

Fig. 1. Thermal analyses of the $Zn_xNi_{1-x}WO_4$ powder precursors ($x = 0$, 0.2, 0.4, 0.6, 0.8 and 1.0), after heat treatment at 350 °C for 12 h, in oxygen atmosphere. (a) TG and (b) DTA.

two steps, the first one being related to the elimination of water and adsorbed gases whilst the second one being related to the exothermic combustion of the organic material, leading to the formation of CO_2 and H_2O.

Fig. 2 displays the DTG peak temperatures from which it is apparent that an increase in the zinc content of the pigments increased the temperature of combustion, indicating that the presence of zinc leads to more stable organic compounds. This result was observed from the TG and DTA curves, which show that zinc-rich samples displayed greater mass loss and more exothermic peaks. These findings indicate the difficulty of eliminating carbon from the samples during calcination at 350 °C. The same behavior has been observed for other zinc-containing compounds [15].

In terms of calcination between 400 and 700 °C, highest crystallinity was observed for the samples which had been heat treated at 700 °C, which can be attributed to the substantial elimination of carbon. All subsequent discussion will be confined to the analysis of samples calcined at 700 °C.

Fig. 3 shows the IR spectra of the $Zn_xNi_{1-x}WO_4$ pigments, heat treated at 700 °C. Band assignments are presented in Table 1.

For wolframite, the total representation of the *P*2/*c* unit cell contained 18 Raman-active modes ($8A_g + 10B_g$), 15 infrared-active modes ($7A_u + 8B_u$), and 3 acoustic vibrational modes ($A_u + 2B_u$) [16].

Hanuza et al. reported the internal ν_1–ν_4 modes of tungstate anions in the wolframite structure (Table 1). Moreover, the wolframite structure has a relatively high degree of condensation of oxygen atoms around the W^{6+} ions and dense packing of the coordination polyhedra in the unit cell. The resulting coordination number (CN) is 6 because the tungstate ions are additionally connected to each other by means of intermolecular $W^O{}_OW$-type interactions. The characteristic vibrational bands corresponding to this structural fragment appeared at 500–700 and 220–280 cm^{-1} regions and are assignable to the stretching and bending modes of the $W^O{}_OW$ unit, respectively [17,18]. These findings agree with those of Frost et al., who consider that the condensed octahedra of the wolframite group can be

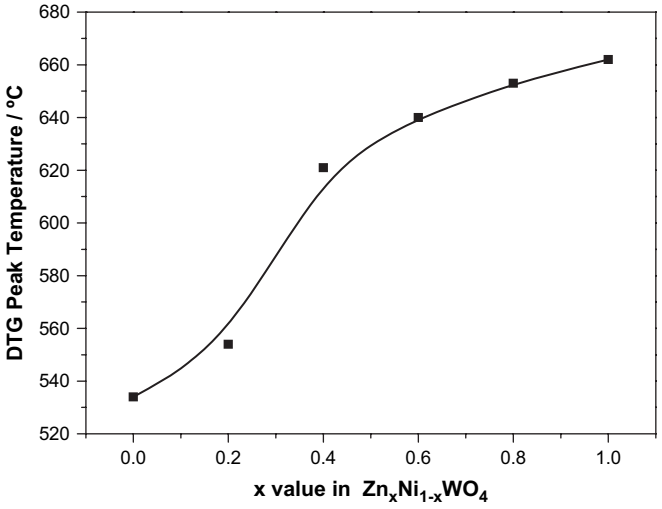

Fig. 2. DTG peak temperature of $Zn_xNi_{1-x}WO_4$, as a function of the zinc amount.

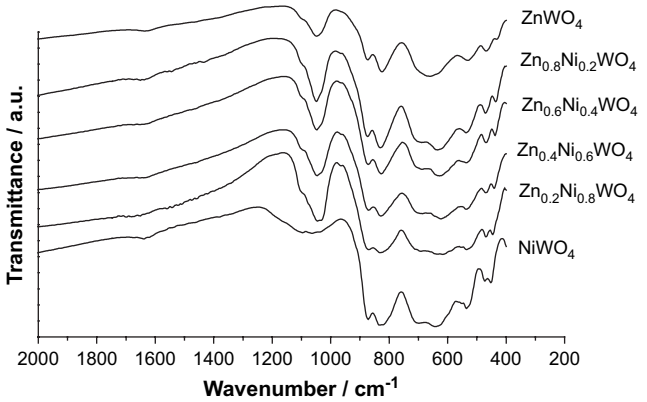

Fig. 3. Infrared spectra of the $Zn_xNi_{1-x}WO_4$ pigments, heat treated at 700 °C wolframite.

clearly distinguished from the isolated tetrahedra of the scheelite group by an infrared band at 600 cm^{-1} [19]. Redfern reported absorptions at 880, 830 and 710 cm^{-1} for $ZnWO_4$, which were assigned to internal vibrations of the distorted WO_6 octahedra; this worker also found phonon resonances at 546, 612, 622, 724, 804, 883, 1112 and 1191 cm^{-1}. Using absorption spectra obtained at different temperatures, Redfern concluded that resonances at 1112 and 1191 cm^{-1} can be assigned to ZnO_6 internal vibrations [16].

The literature data [16–20] were compared to the bands observed in the present work (Table 1). For the majority of the bands, no meaningful variation was observed when Zn^{2+} was substituted for Ni^{2+}. Only two bands present a variation in their positions namely the $\nu_{as}(WO_6)^{6-}$ and $\nu(W^O{}_OW)$ stretching modes between 660 and 696 cm^{-1} and the $\delta_s(WO_6)^{6-}$ bending mode, which varied from 432 to 451 cm^{-1}. These bands are probably influenced by the bonding amongst $[WO_6]^{6-}$ and the $[ZnO_6]^{10-}$ or $[NiO_6]^{10-}$ octahedra.

Small bands at around 1640 cm^{-1} were still observed, being assigned to the asymmetric stretching of the COO^- group for a monodentate complex in esters [20], indicating that carbon elimination was not complete. The pigments also showed one band between 1040 and 1080 cm^{-1}, ascribed to hydroxyl groups [20] that were probably present on the surface of the material. This band was more defined for the zinc-containing samples.

X-ray diffraction was used to study the effect of the modifier ion on the structure of the pigments. Thus, Fig. 4 depicts the XRD patterns of the $Zn_xNi_{1-x}WO_4$ pigments, in which $x = 0$, 0.2, 0.4, 0.6, 0.8 and 1.0, calcined at 700 °C. Monoclinic wolframite was the main phase observed in all cases, but the patterns indicated the presence of secondary phases, NiO, WO_3, ZnO and ZrO_2, in some samples, which can be related either to the synthesis, in the case of NiO, WO_3 and ZnO, or to the milling process, in the case of ZrO_2.

The relative crystallinity (RC) was calculated according to Eq. (1):

$$RC = \frac{I - I_o}{I_{100} - I_o} \times 100\% \quad (1)$$

Table 1
Peak positions and attributions of the infrared absorption spectra of the $Zn_xNi_{1-x}WO_4$ pigments, heat treated at 700 °C

x Value in $Zn_xNi_{1-x}WO_4$						Assignment	Ref.
1	0.8	0.6	0.4	0.2	0		
1637_s	1650_s	1651_s	1629_s	1650_{vs}	1639_s	COO^- Monodentate	[20]
1100_{sh}	1100_{sh}	1100_{sh}	1100_{sh}	1100_{sh}	1095	MeO_6	[16]
1047	1049	1049	1047	1045	1065	MeO_6	[16]
874	874	872	870	870	872	$\nu_s(WO_6)^{6-}$	[18]
825	831	827	829	831	833	$\nu_{as}(WO_6)^{6-}$ and $\nu(W^O{}_OW)$ – st	[18]
660	688	687	687	690	696	$\nu_{as}(WO_6)^{6-}$ and $\nu(W^O{}_OW)$ – st	[18]
–	634	627	625	617, 634	642	$\nu_{as}(WO_6)^{6-}$ and $\nu(W^O{}_OW)$ – st	[18]
530	536	536	536	536	536	$\nu_{as}(WO_6)^{6-}$ and $\nu(W^O{}_OW)$ – st	[18]
469	471	469	469	469	473	$\nu_{as}(WO_6)^{6-}$ and $\nu(W^O{}_OW)$ – st	[18]
432_s	436	438	442	445	451	$\delta_s(WO_6)^{6-}$ – bd	[18]

Band characteristics: s – small, vs – very small, sh – shoulder, br – broad. Vibration modes: st – stretching mode, bd – bending mode. The peak wavenumbers are presented in cm^{-1}.

where I_{100} is the intensity of the $(\bar{1}11)$ peak of the most crystalline sample; I_o is the intensity of the $(\bar{1}11)$ peak of the less crystalline sample and I is the intensity of the $(\bar{1}11)$ peak of other samples.

Fig. 5 shows the relative crystallinity of the $Zn_xNi_{1-x}WO_4$ pigments, heat treated at 700 °C, as a function of zinc content in $Zn_xNi_{1-x}WO_4$. A tendency of decreasing relative crystallinity was observed which indicates that crystallization of Zn^{2+}-rich samples was more difficult due to the increased stability of the organic compounds during the synthesis, as observed by thermal analysis.

Fig. 6 shows the FWHM values of the $(\bar{1}11)$ peak of the XRD patterns, displayed in Fig. 3. The nickel-rich samples displayed lower, long range organization than the zinc-rich pigments probably due to the higher covalent character of Ni^{2+}, compared to Zn^{2+}, leading to higher distortion of the unit cell. It was also observed that the samples displaying equimolar composition had the highest long range order, giving rise to an U-shaped curve. Upon Zn^{2+} addition, higher short range disorder occurs, as two different cations occupy the same octahedral site; the defects formed are presented in Eq. (2). It may be observed that 6-fold Zn^{2+} polyhedra were formed, besides the usual 6-fold Ni^{2+} polyhedra and 6-fold W^{6+} polyhedra. As a consequence, order–disordered phases are formed, with three different cations in octahedral coordination.

$$ZnO \xrightarrow{NiWO_4} Zn^x_{Ni} + O^x_O \quad (2)$$

Table 2 shows the lattice parameters, a, b, c and β, of the $Zn_xNi_{1-x}WO_4$ pigments, calculated from the XRD patterns previously presented. The c parameter had no meaningful variation, while the b parameter increased with increasing x values. The same tendency was observed for the volume of the unit cell, indicating that this system does not obey Vegard's law. The same tendency was revealed from the FWHM analysis (Fig. 6). Thus, such variation may be related to the higher

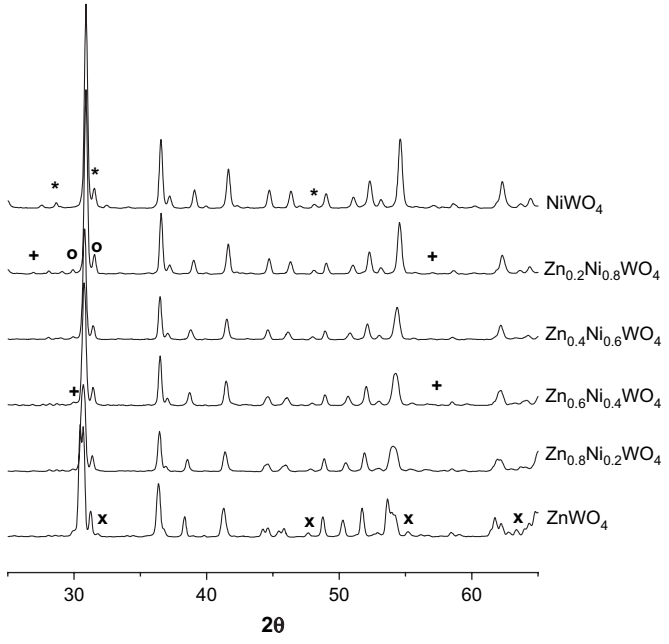

Fig. 4. X-ray diffraction patterns of the $Zn_xNi_{1-x}WO_4$ pigments, heat treated at 700 °C. * – NiO, + – WO_3, x – ZnO and ° – ZrO_2. All the other diffraction peaks refer to monoclinic.

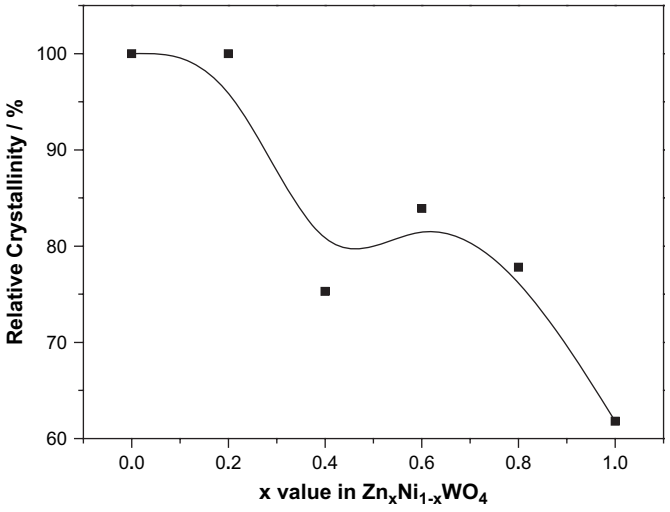

Fig. 5. Relative crystallinity in the $Zn_xNi_{1-x}WO_4$ pigments, heat treated at 700 °C, as a function of the zinc content in $Zn_xNi_{1-x}WO_4$.

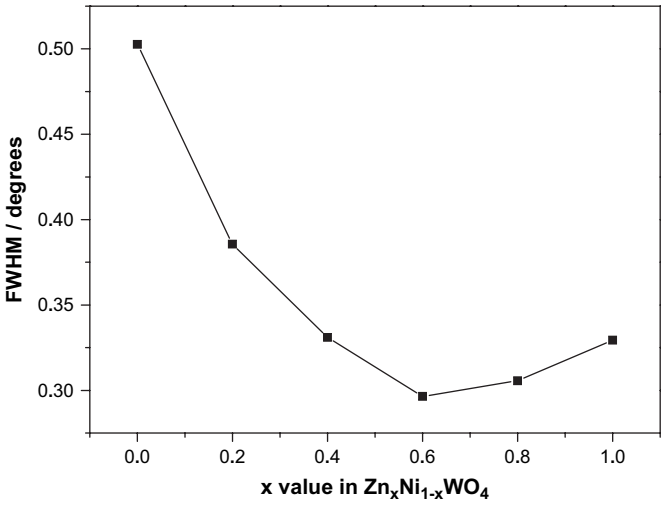

Fig. 6. FWHM of the ($\bar{1}11$) peak of the XRD patterns of the $Zn_xNi_{1-x}WO_4$ pigments, heat treated at 700 °C, as a function of the zinc content.

short range disorder, observed when two modifiers are present in the unit cell.

Table 3 presents the CIE$L^*a^*b^*$ colorimetric data for the $Zn_xNi_{1-x}WO_4$ pigments [12]. As the Ni^{2+} content increased, higher positive values of b^* accrued (yellow color), while the a^* values remained small and positive (red color). Furukawa et al. synthesized light yellow colored pigments of $Ce_{1-x}Z_{-x}W_2O_8$ stoichiometry with b^* values of 47–68 and L^* values of 79–81 [3]. The disadvantage of these pigments was the use of a rare earth as chromophore, making them expensive.

The appearance of yellow color in the synthesized pigments can be ascribed to the absorption of its complementary color, blue, by these pigments [21]. The absorption spectra of the $Zn_xNi_{1-x}WO_4$ pigments are presented in Fig. 7. The different absorption spectra were separated into the discrete absorption Gaussian bands with the aid of the Peak Fit program, as exemplified in the case of $Zn_{0.8}Ni_{0.2}WO_4$ pigments, shown in Fig. 8. Deconvolution data are presented in Table 4.

The $ZnWO_4$ pigment presents two absorbance bands of low intensity centered at 1.65, 2.19 and 2.73 eV. As both bands are located in the visible region, the Ni-free pigment is not completely white, as shown by its low a^* and b^* colorimetric parameters. One band of high intensity was observed, in the ultraviolet region, being centered at 3.46 eV. Hanuza et al. [17] evaluated the visible spectra of single crystals of wolframites of $NaCr(WO_4)_2$ and $LiCr(WO_4)_2$ stoichiometry and

Table 2
Structural parameters of the $Zn_xNi_{1-x}WO_4$ samples, heat treated at 700 °C

Sample	a (Å)	b (Å)	c (Å)	β (°)	Volume (Å^3)
$NiWO_4$	4.60	5.67	4.93	89.90	128.6
$Zn_{0.2}Ni_{0.8}WO_4$	4.60	5.68	4.94	89.75	129.0
$Zn_{0.4}Ni_{0.6}WO_4$	4.65	5.69	4.92	89.73	130.0
$Zn_{0.6}Ni_{0.4}WO_4$	4.70	5.69	4.92	90.82	131.6
$Zn_{0.8}Ni_{0.2}WO_4$	4.67	5.70	4.90	88.61	130.5
$ZnWO_4$	4.69	5.72	4.93	90.57	132.4

Table 3
CIE$L^*a^*b^*$ colorimetric data for the $Zn_xNi_{1-x}WO_4$ pigments

Pigment	L^*	a^*	b^*
$NiWO_4$	68.42	3.84	31.68
$Zn_{0.2}Ni_{0.8}WO_4$	65.92	2.38	28.09
$Zn_{0.4}Ni_{0.6}WO_4$	62.55	2.29	25.55
$Zn_{0.6}Ni_{0.4}WO_4$	67.91	2.63	26.27
$Zn_{0.8}Ni_{0.2}WO_4$	74.06	2.73	25.04
$ZnWO_4$	79.81	0.38	6.35

observed the characteristic energy features associated with the maxima of $^4A_2$–$^4T_1$ (^4P) and $^4A_2$–$^4T_2$ transitions, at about 3.4 and 1.7 eV, respectively. These bands were also observed in the synthesized pigments herein, being centered at 3.46 and 1.65 eV, respectively. Hanuza et al. [17] also observed bands at 1.8 and 2.5 eV, assigned to the $^4A_2$–^2E and $^4A_2$–$^4T_1$ (^4F) transitions; these transitions were not observed in this work.

The $^4A_2$–$^4T_1$ (^4P) transition was observed in all samples of high intensity and with a small variation in the band position (3.43–3.48 eV). Three other bands were observed in Ni-containing pigments namely, a low intensity, near IR band <1.65 eV, a second band of varying intensity in the range 2.00–2.23 eV and a third band of highest intensity in the range 2.71–2.78 eV (21 800–22 400 cm^{-1}). Thus, the maximum absorption of these bands takes place in the blue region, from 458 to 446 nm and the pigment color perceived therefore corresponds to yellow, the complementary color of blue.

In NiO, as in the $Zn_xNi_{1-x}WO_4$ pigments, the Ni^{2+} ions are octahedrally surrounded by O^{2-} ions, which provide a partial lifting of the degeneracy of the $3d^8$ states of the Ni^{2+} ions. The d_{z^2} and $d_{x^2-y^2}$ orbitals (e_g states) are energetically separated from the d_{xy}, d_{xz} and d_{xz} orbitals (t_{2g} states). The ground state of the ions is of $^3A_{2g}$ symmetry ($t_{2g}^6e_g^2$) and several excited states with triplet and singlet characters have been predicted theoretically [22].

Mackrodt and Noguera [23] studied the bulk excitation energies in NiO; different literatures give energy values of about

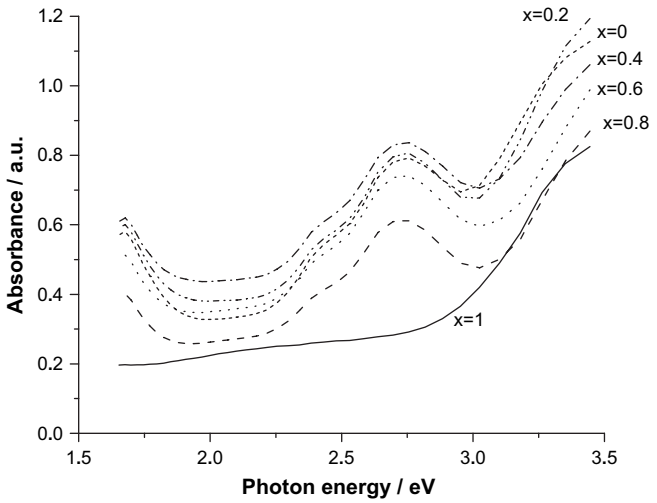

Fig. 7. Optical spectra of the $Zn_xNi_{1-x}WO_4$ pigments, calcined at 700 °C.

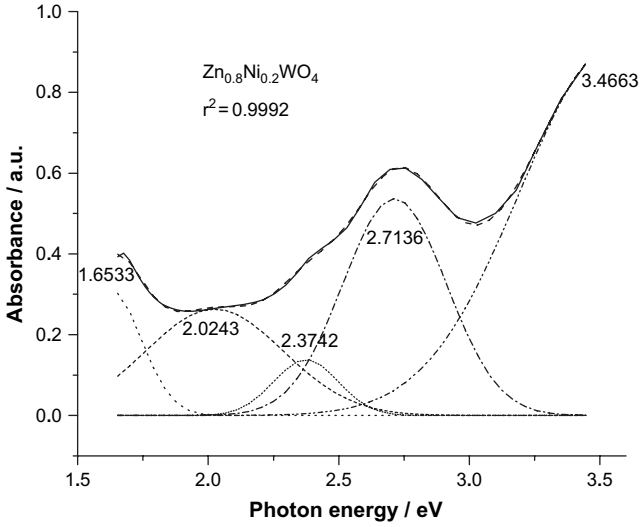

Fig. 8. Example of peak deconvolution for the sample $Zn_{0.8}Ni_{0.2}WO_4$.

2.75 eV for a $^3A_{2g} \rightarrow {}^3T_{1g}$ ($t_{2g}^6 e_g^2 \rightarrow t_{2g}^5 e_g^3$) transition for the octahedrally coordinated Ni^{2+} cations. These authors calculated such $d \rightarrow d$ transition as 2.71 eV, using first-principles Hartree–Fock calculations, which is in agreement with the reported data. Fromme et al. [22], for the same NiO, reported a similar value of 2.80 eV. These results are also in agreement with the present work, which shows the $^3A_{2g} \rightarrow {}^3T_{1g}$ transition in the range 2.71–2.78 eV.

Table 4
Deconvolution of the absorption spectra of the $Zn_xNi_{1-x}WO_4$ pigments, calcined at 700 °C

Sample	Peak	Center (eV)	Peak intensity (arb. units)	FWHM (eV)
$NiWO_4$ ($r^2 = 0.9967$)	1	1.64	0.30	0.28
	2	2.22	0.33	2.50
	3	2.72	0.45	0.54
	4	3.43	0.95	0.63
$Zn_{0.2}Ni_{0.8}WO_4$ ($r^2 = 0.9972$)	1	1.51	0.70	0.65
	2	2.13	0.26	0.55
	3	2.76	0.78	0.70
	4	3.19	0.21	0.26
	5	3.47	1.13	0.44
$Zn_{04}Ni_{0.6}WO_4$ ($r^2 = 0.9970$)	1	1.58	0.39	0.36
	2	2.06	0.42	1.06
	3	2.75	0.65	0.60
	4	3.47	1.04	0.67
$Zn_{0.6}Ni_{0.4}WO_4$ ($r^2 = 0.9978$)	1	1.65	0.19	0.21
	2	2.00	0.35	2.04
	3	2.78	0.50	0.60
	4	3.18	0.17	0.28
	5	3.48	0.89	0.43
$Zn_{0.8}Ni_{0.2}WO_4$ ($r^2 = 0.9992$)	1	1.65	0.30	0.28
	2	2.02	0.26	0.62
	3	2.37	0.14	0.29
	4	2.71	0.54	0.47
	5	3.47	0.88	0.88
$ZnWO_4$ ($r^2 = 0.9998$)	1	1.65	0.17	0.88
	2	2.19	0.14	0.62
	3	2.73	0.23	0.75
	4	3.46	0.81	0.71

Dondi et al. [24] studied the absorbance of Ni-doped rutile and reported, in the red-NIR region, a peak at 13 500 cm^{-1} (1.67 eV), which could be ascribed either to the unusual co-presence of Ni^{3+} e.g. $^4T_1(^4F) \rightarrow {}^4T_2(^4F)$ or to a considerable splitting of the Ni^{2+} ν_2 transition, as wide as 1190–1410 cm^{-1}, related to the [TiO_6] octahedra distortion. The lowest energy absorption band observed in the present work matches the energy values reported by Dondi et al. and may be also related either to the co-presence of Ni^{3+} or more probably to the distortion of the [WO_6] octahedra in the wolframite structure, as soon as this band is already observed in $ZnWO_4$.

Llusar et al. used an ab initio model for the calculation of the electronic spectrum of Ni^{2+}-doped MgO [25] and reported spin-free ligand field absorption energies of 13 400, 21 550 and 28 300 cm^{-1} (1.66, 2.67 and 3.51 eV) for the transitions $^3A_{2g} \rightarrow a^1E_g$, $^3A_{2g} \rightarrow a^1T_{2g}$ and $^3A_{2g} \rightarrow {}^1T_{1g}$, respectively. It should be stressed that, although in a different ligand field, the values obtained in the present paper agree with the energies reported by these authors.

4. Conclusions

$Zn_xNi_{1-x}WO_4$ pigments of wolframite structure were obtained, at low temperature, using a polymeric precursor method. Increase in the zinc content increased the temperature of organic material combustion, making crystallization more difficult. Nickel-rich samples displayed lower, long range organization than zinc-rich pigments and samples displaying a nearly equimolar composition had the lowest short range order.

The colorimetric data showed increased brightness with increasing zinc content. As the Ni content increased, higher b^* values were recorded, while the a^* value remained small, giving rise to stronger yellow colored pigments.

The absorption spectra of the $Zn_xNi_{1-x}WO_4$ pigments separated into discrete absorption Gaussian bands, showing absorption bands centered in the range of 2.71–2.78 eV, due to [NiO_6] transitions. An absorption band due to [WO_6] was observed between 3.43 and 3.48 eV. Thus, the maximum absorption of such band takes place in the blue region, from 458 to 446 nm, and the pigment color perceived corresponds to yellow, the complementary color of blue, as pointed out in the colorimetric results.

References

[1] Zhang H, Feng M, Liu F, Liu L, Chen H, Gao H, et al. Structures and defects of WO_{3-x} nanorods grown by in-situ heating tungsten filament. Chemical Physics Letters 2004;389:337–41.
[2] Gotic M, Ivanda M, Popovic S, Music S. Synthesis of tungsten trioxide hydrates and their structural properties. Materials Science and Engineering 2000;B77(2):193–201.
[3] Furukawa S, Masui T, Imanaka N. Synthesis of new environment-friendly yellow pigments. Journal of Alloys and Compounds 2006;418(1–2):255–8.

[4] Diot N, Larcher O, Marchand R, Kempf JY, Macaudiere P. Rare-earth and tungsten oxynitrides with a defect fluorite-type structure as new pigments. Journal of Alloys and Compounds 2001;323:45–8.
[5] Kloprogge JT, Weier ML, Duong LV, Frost RL. Microwave-assisted synthesis and characterisation of divalent metal tungstate nanocrystalline minerals: ferberite, hübnerite, sanmartinite, scheelite and stolzite. Materials Chemistry and Physics 2004;88(2–3):438–43.
[6] Kuzmin A, Purans J. Local atomic and electronic structure of tungsten ions in AWO_4 crystals of scheelite and wolframite types. Radiation Measurements 2001;33(5):583–6.
[7] Zou Z, Ye J, Arakawa H. Photophysical and photocatalytic properties of In MO_4 ($M = Nb^{5+}$, Ta^{5+}) under visible light irradiation. Materials Research Bulletin 2001;36:1185–93.
[8] Errandonea D, Somayazulu M, Hausermann D. Phase transitions and amorphization of $CaWO_4$ at high pressure. Physical Status Solidi B – Basic Research 2003;235(1):162–9.
[9] Sen A, Pramanik P. A chemical synthetic route for the preparation of fine-grained metal tungstate powders (M = Ca, Co, Ni, Cu, Zn). Journal of the European Ceramic Society 2001;21(6):745–50.
[10] Ciaco FRC, Pontes FM, Pinheiro CD, Leite ER, Lazaro SR, Varela JA, et al. O papel dos modificadores de rede na produção da fotoluminescência no $CaWO_4$. Cerâmica 2004;50(313):43–9.
[11] Kakihana M, Yoshimura M. Synthesis and characteristics of complex multicomponent oxides prepared by polymer complex method. Bulletin of the Chemical Society of Japan 1999;72(7):1427–43.
[12] Gouveia DS, Soledade LEB, Paskocimas CA, Longo E, Souza AG, Santos IMG. Color and structural analysis of $Co_xZn_{7-x}Sb_2O_{12}$ pigments. Materials Research Bulletin 2006;41(11):2049–56.
[13] Pereira LG, Araújo AS, Souza MJB, Pedrosa AMG, Cássia-Santos MR, Santos IMG, et al. MoO_3-based HDS catalyst obtained by the polymeric precursor method. Materials Letters 2006;60(21–22):2638–41.
[14] Souza SC, Santos IMG, Silva MRS, Cássia-Santos MR, Soledade LEB, Souza AG, et al. Influence of pH on iron doped Zn_2TiO_4 pigments. Journal of Thermal Analysis and Calorimetry 2005;79(2):451–4.
[15] Gouveia DS, Rosenhaim R, Lima SJG, Longo E, Souza AG, Santos IMG. The characterization of $Co_xZn_{7-x}Sb_2O_{12}$ spinel obtained by the Pechini method. Materials Research 2005;8(2):213–9.
[16] Redfern SAT. Hard-mode infrared study of the ferroelastic phase-transition in $CuWO_4$–$ZnWO_4$ mixed-crystals. Physical Review 1993;B48(9):5761–5.
[17] Hanuza J, Maczka M, Hermanowicz K, Deren PJ, Strek W, Folcik L, et al. Spectroscopic properties and magnetic phase transitions in scheelite M(I)Cr(MoO_4)(2) and wolframite M(I)Cr(WO_4)(2) crystals, where M(I) = Li, Na, K, and Cs. Journal of Solid State Chemistry 1999;148(2):468–78.
[18] Hanuza J, Maczka M, Van der Mass JH. Vibrational properties of double tungstates of the M(I)M(III)(WO_4)(2) family (M(I) = Li, Na, K–M(III) = Bi, Cr). Journal of Solid State Chemistry 1995;117(1):177–88.
[19] Frost RL, Duong L, Weier M. Raman microscopy of selected tungstate minerals. Spectrochimica Acta Part A 2004;60(8–9):1853–9.
[20] Nakamoto K, editor. Infrared and Raman spectra of inorganic and coordination compounds. New York: John Wiley and Sons; 1980.
[21] Nassau K, editor. The physics and chemistry of color: the fifteen causes of color. New York: John Wiley & Sons; 1983. p. 12.
[22] Fromme B, Schmitt M, Kisker E, Gorschlüter A, Merz M. Spin-flip low-energy electron-exchange scattering in NiO(100). Physical Review 1994;B50(3):1874–8.
[23] Mackrodt WC, Noguera C. Bulk and (100) surface d > d excitation energies in NiO from first-principles Hartree–Fock calculations. Surface Science 2000;457(1–2):386–90.
[24] Dondi M, Cruciani G, Guarini G, Matteucci F, Raimondo M. The role of counterions (Mo, Nb, Sb, W) in Cr-, Mn-, Ni- and V-doped rutile ceramic pigments – part 2: colour and technological properties. Ceramics International 2006;32(4):393–405.
[25] Llusar R, Casarrubios M, Barandiarán Z, Seijo L. Ab initio model potential calculations on the electronic spectrum of Ni^{2+}-doped MgO including correlation, spin-orbit and embedding effects. Journal of Chemical Physics 1996;105(13):5321–30.